International Journal of Information Acquisition
Vol. 2, No. 1 (2005) 63–76

MODELING A THERMAL IMAGING PROCESS IN AN IMPACT DAMAGED COMPOSITE STRUCTURE

M. Z. ISKANDARANI
Faculty of Science and Information Technology
Al-Zaytoonah University, Amman, Jordan

N. F. SHILBAYEH
Faculty of Computer Science and Information Technology
Applied Science University, Amman, Jordan

Received 19 August 2004
Accepted 2 February 2005

An innovative NDT (non-destructive testing) technique for interrogating materials for their defects has been developed successfully. The technique has a novel approach to data analysis by employing intensity, RGB signal re-mix and wavelength variation of a thermally generated IR-beam onto the specimen under test which can be sensed and displayed on a computer screen as an image. Specimen inspection and data analysis are carried out through pixel level re-ordering and shelving techniques within a transformed image file using a sequence grouping and regrouping software system, which is specifically developed for this work. The interaction between an impact damaged RIM composite structure and thermal energy is recorded, analyzed, and modeled using an equivalent Electronic circuit. Effect of impact damage on the integrity of the composite structure is also discussed.

Keywords: Non-destructive testing; defect detection; thermal imaging; infrared, image slicing.

1. Introduction

Most NDT techniques available at present suffer from limitations imposed by detecting hardware, interpreting software or both. These limitations such as accuracy, resolution, depth of detection, type of detected defect, instrument portability, data repeatability, and material properties have been under investigation for some considerable time [Dillenz *et al.*, 2003; Favro *et al.*, 2000; Galmiche *et al.*, 2000; Maldague *et al.*, 2002; Huang *et al.*, 2004].

The efforts were mainly directed towards sophistication of the detecting devices and the processing system. In addition, the most successful NDT systems are extremely costly and time consuming in the detection and analysis.

Thermal non-destructive testing can be employed to detect inclusions and flaws in polymeric composite laminates by demonstrating the difference in their heat transfer properties from the undamaged structure. When external heat is applied, the presence of defects affects the normal heat flow pattern of the structure. If this heat propagation is altered sufficiently, a temperature distribution profile can be realized. This distribution is then related to the existence of a flaw in the material. Infrared devices and sensitive coatings (e.g. liquid crystals) are two of the most practical temperature detecting systems that may be used in developing test devices [Dillenz *et al.*, 2003; Favro *et al.*, 2000].

Thermography is essentially a technique whereby infrared radiation from the sample is captured and subsequently converted into an electrical signal generating a real-time thermal image.

Thermal imaging information can be obtained regarding the following parameters:

(i) Thickness variation.
(ii) Material content homogeneity.
(iii) Porosity.
(iv) Defect dimensions.

In this paper, the process of using Time Video Thermography (TVT) to detect impact damage in composite structures is modeled. This technique employs a low-energy pulse to strike the structure under test over a period. An electronic model is presented to explain and account for the response of the chosen composite structure to thermal energy.

2. Experimental Setup

2.1. *System arrangement*

The chosen composite was a laminate made by resin injection molding (RIM) to produce 5 mm thick samples that contain five layers of U750/450 Vetrotex continuous mat glass fiber impregnated with 65.4% 1153/72/A epoxy resin from SHELL mixed with 50 g of 1153/172/B hardener at 4:1 ratio.

The testing set-up for RIM samples are shown in Fig. 1. The equipment used comprised a tungsten filament light bulb rated at 125 watts with an AGEMA 870 Infrared Camera. Images are captured in digitally real time and analyzed using MICROEYE IC MK2 hardware and software.

2.2. *Data acquisition system*

2.2.1. *Background*

Composites are increasingly being used as structural materials. One of the major advantages of composite materials is their ability to be tailored to meet certain applications. Thus, a particular type of fiber and matrix can be used to produce components acquiring different lay-ups, thicknesses, and volume fractions. This implies that a defect, which is considered critical in one component, might be totally acceptable in another. Hence, setting quality control and inspection standards is a very complex task, and is not made any simpler or economical due to the different NDT techniques, each of which is capable of detecting certain defects. Together with employing standard but variable interpretation methods, efforts have been directed towards balancing the cost and complexity of an inspection technique against the quality of information

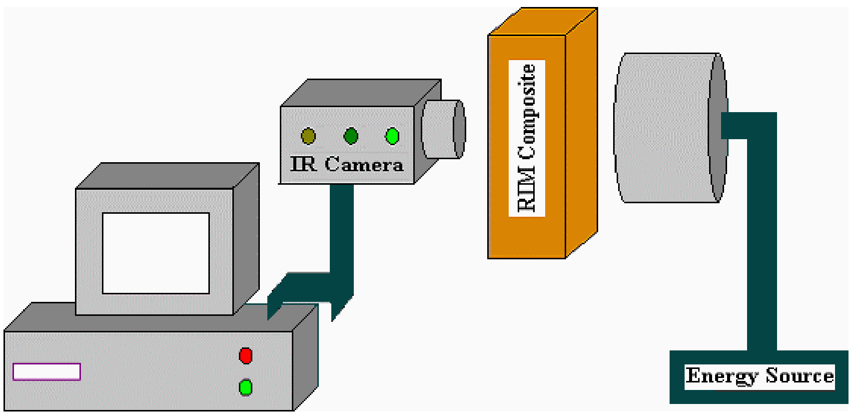

Fig. 1. TVT testing system.

obtained its flexibility in detecting various types of defects.

As a solution to the problems associated with NDT applications, there is a need to establish an intelligent analysis system coupled to a portable detection environment that unifies all different types of inputs and automatically considers various fiber/matrix combinations which leads to elimination of any ambiguity regarding defect severity and its effect on the component under consideration. This suggests the use of an imaging system together with smart classification techniques.

The automated image capturing system possesses the following main characteristics:

(i) The ability to extract important information from a background of irrelevant details.
(ii) The capacity to learn from experience and apply its knowledge to new situations.
(iii) Capable of correlating and predicting from distorted or lost data files.

2.2.2. *System design*

Based on the characteristics described above, a smart classification system with intelligent knowledge base is designed. This system operates on the principles of image slicing and nearest neighbor classifier [Spicer *et al.*, 1999; Busse *et al.*, 1992; Busse, 1994; Wu *et al.*, 1996; Balageas & Levesque, 1998]. Our classifier differs from the known classifiers in that it operates on the wavelength of the converted image pixels and their intensities, as shown in Fig. 2.

2.2.3. *System processing and interpretation*

Figure 3 illustrates the process that the image goes through from the capturing stage into

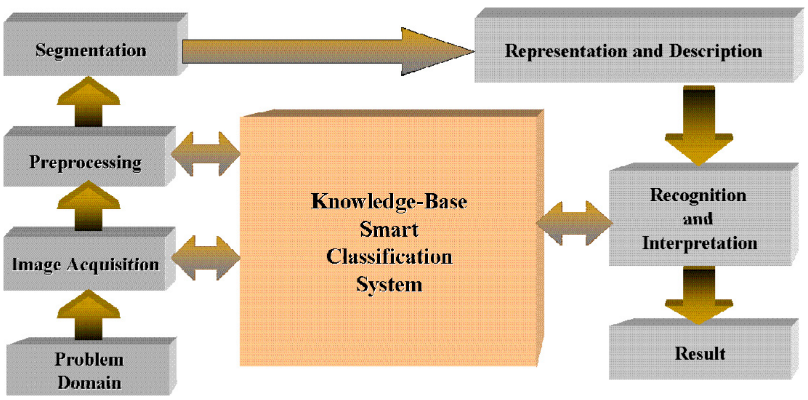

Fig. 2. Block diagram of the image acquisition system.

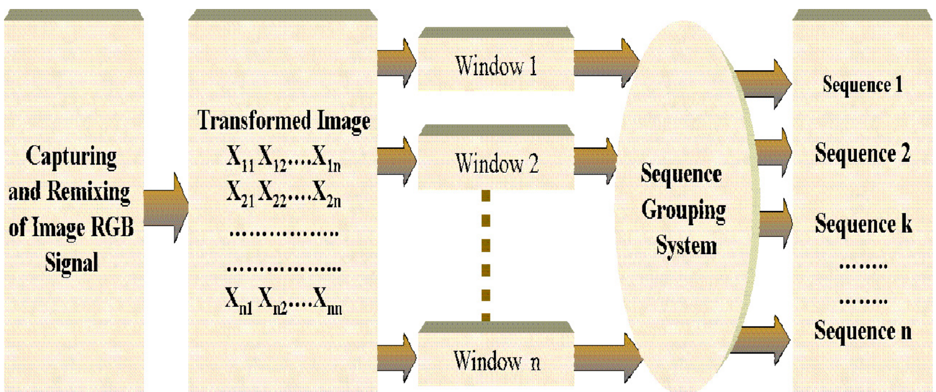

Fig. 3. Overall image analysis and interpretation system.

interpretation after re-mixing its RGB signal by first converting it to numerical format before passing it through various windows or software gates, each of which will extract information from the converted image within a particular wavelength range which the principle of grouping is based on pixel value that occupies a certain level (Microstates). The data is then grouped into five main sequences per wavelength and image pixel values are stacked relative to their amplitude and phase. Such a grouping will statistically gather equivalent pixel values (neighborhood grouping) and will place pixel numbers within the five main sequences in what we call Macro states. The five main Macro states are divided as follows:

(i) Sequence 0–49,
(ii) Sequence 50–100,
(iii) Sequence 101–150,
(iv) Sequence 151–200,
(v) Sequence 201–250.

This operation is followed by a re-grouping process within each of the five sequences and a comparison of re-grouped values are established with ratios to establish the level and type of damage taking into considerations the theoretical and mathematical model that will measure how close the obtained results to theoretical considerations. Such a process of grouping and re-grouping comes after a process of remixing of the RGB signal in order to obtain the optimum ratios of RGB colors so that to easily unmask the existence, location, and effect of a damage on the integrity of the composite structure.

It is worth mentioning that in our TVT system the capturing of the signal is time bounded to avoid the swamping effect that would result from subjecting the composite structure under test to an excess of energy which would result in masking the existence of damage within the structure.

3. Mathematical Modeling

Based on the previous discussion, a model is developed to account for the response of such composite structure to thermal pulses.

Figure 4 illustrates this model, which is based on a closed loop feedback control system.

From the diagram, we have:

$$e = x - \beta \cdot y, \tag{1}$$

$$y = \alpha \cdot e, \tag{2}$$

$$\left(\frac{x}{y}\right) = \left(\frac{1 + \alpha \cdot \beta}{\alpha}\right) = \left(\frac{1}{k}\right). \tag{3}$$

Assuming minimum loss, $\alpha \to 1$:

$$k = \left(\frac{1}{1 + \beta}\right), \tag{4}$$

where

$$\beta = \left(\frac{t_d}{t_r}\right). \tag{5}$$

By back substitution, we obtain:

$$k = \left(\frac{t_r}{t_d + t_r}\right), \tag{6}$$

where

t_r: Reference response time,
t_d: Defect (damaged area) response time,
k: Response factor.

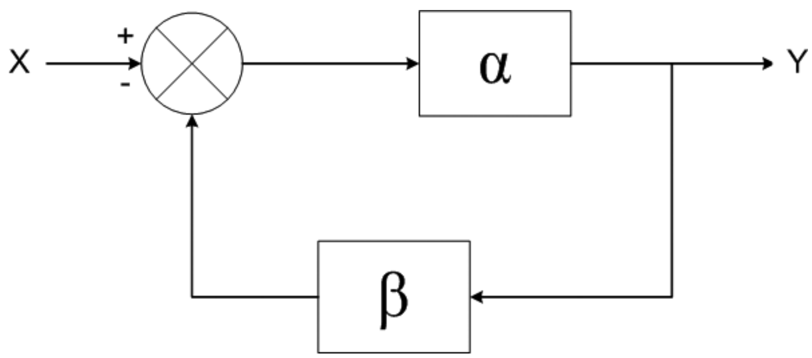

Fig. 4. Closed loop feedback diagram representing component response to thermal pulses.

Equation (6) indicates that the response factor for a composite structure can be used and correlated to the number of regrouped pixels to judge the state of the structure under test. Three specific cases can be realized and verified.

$\boldsymbol{t_r \gg t_d}$.

Here the structure is either non-defective or the level of damage is will below the detectable one for which the impact energy is much below the structure threshold. Hence

$$\lim_{t_d \to 0} k = 1. \tag{7}$$

This limit of one is an absolute maximum and if reached (not possible in practice) means a perfect component structure.

$\boldsymbol{t_r \cong t_d}$.

Here the structure is defective with the introduced time delay equivalent to the component original response; hence, it is not critical (localized damage) as to compromise the overall integrity of the component, so

$$\lim_{t_d \to t_r} k = 0.5. \tag{8}$$

$\boldsymbol{t_r \ll t_d}$

In this case, the tested composite is severally damaged and it is serious or critical level, hence

$$\lim_{t_d \to \infty} k = \left(\frac{t_r}{t_d}\right). \tag{9}$$

Equation (9) clearly indicates a total structural failure whereby the excessive damage that is caused to the composite resulted in a very long response time (defect response time, t_d). Such a slow response time when compared to the standard, non-damaged composite response time and as a ratio will result in a near zero response factor (k).

4. Results

Figures 5–8 show the obtained results from a TVT test carried out on 5 mm thick RIM samples. Figure 5 presents the results of an undamaged sample called the reference sample. Figures 6 and 7 show the results of 42 J and 55.6 J impacts on this composite. The images clearly illustrate the concept of energy storage by a defect or damaged part of the composite. In addition, the images show that for the same thickness the larger the impact energy the wider and deeper the affected area. This

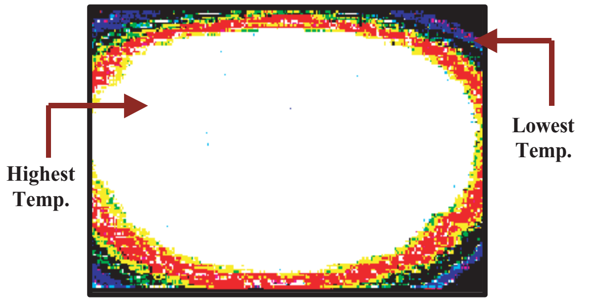

Fig. 5. TVT of an undamaged reference RIM composite.

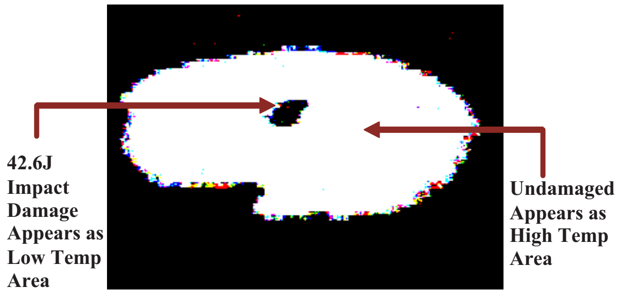

Fig. 6. A thermally charged 5 mm RIM Sample Impacted at 42.6 J.

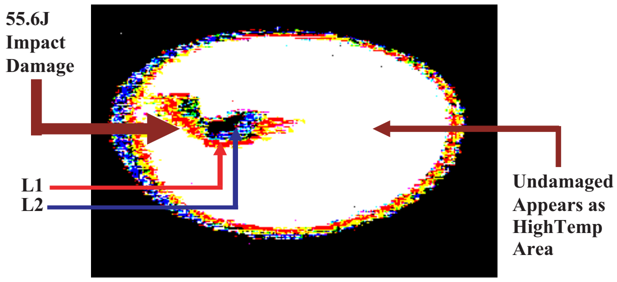

Fig. 7. 5 mm RIM (L1, L2 first two layers to be charged).

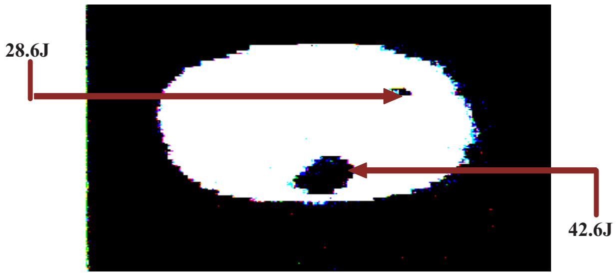

Fig. 8. 5 mm RIM subjected to two impacts.

Table 1. RGB data for Fig. 5.

Color	R	B	G	Color	R	B	G	Color	R	B	G	Color	R	B	G
0	8	16	4	64	24	48	28	128	72	16	252	192	8	240	12
1	136	16	4	65	40	16	180	129	136	16	84	193	8	16	180
2	0	0	128	66	136	240	148	130	248	48	140	194	72	16	236
3	128	0	128	67	248	48	60	131	8	16	52	195	248	112	60
4	0	128	0	68	40	16	172	132	56	240	188	196	248	48	100
5	128	128	0	69	216	240	236	133	216	16	12	197	248	144	236
6	0	128	128	70	56	16	252	134	248	144	100	198	248	144	244
7	192	192	192	71	200	16	4	135	248	16	228	199	8	208	20
8	200	208	220	72	56	16	204	136	72	240	84	200	56	240	84
9	168	240	204	73	248	80	68	137	248	112	132	201	200	16	28
10	8	16	132	74	8	240	4	138	8	176	12	202	248	48	236
11	136	16	132	75	184	16	156	139	24	16	44	203	24	16	252
12	8	144	4	76	248	80	92	140	40	16	204	204	40	16	164
13	136	144	4	77	56	16	212	141	248	80	116	205	248	48	108
14	8	144	132	78	248	80	84	142	248	48	124	206	248	144	148
15	200	208	196	79	248	80	100	143	248	48	228	207	248	112	220
16	8	16	12	80	248	16	236	144	8	80	28	208	248	112	228
17	24	16	12	81	72	240	76	145	152	16	76	209	248	176	236
18	24	16	20	82	72	16	204	146	8	80	12	210	248	48	252
19	8	16	20	83	184	16	148	147	248	16	132	211	88	240	172
20	232	240	236	84	248	80	108	148	248	l12	140	212	104	240	172
21	232	240	244	85	248	112	116	149	56	16	180	213	152	16	92
22	24	16	28	86	248	80	124	150	168	16	164	214	168	16	84
23	248	240	236	87	248	16	244	151	56	240	68	215	184	16	20
24	8	16	28	88	248	176	252	152	152	16	84	216	248	16	4
25	248	240	244	89	72	16	196	153	184	16	4	217	120	16	212
26	24	16	4	90	168	16	156	154	248	48	220	218	40	16	228
27	232	240	252	91	248	80	132	155	8	80	20	219	120	240	124
28	248	240	252	92	248	112	252	156	8	16	196	220	88	240	188
29	40	16	12	93	8	208	4	157	40	16	36	221	88	16	180
30	232	240	228	94	120	16	4	158	72	240	172	222	88	16	156
31	40	16	20	95	120	16	92	159	136	16	76	223	72	16	28
32	24	16	36	96	136	240	156	160	248	144	116	224	136	16	148
33	8	16	36	97	152	16	4	161	248	80	220	225	8	16	164
34	8	48	12	98	248	48	84	162	24	16	180	226	136	16	60
35	40	16	4	99	72	16	212	163	104	240	164	227	8	16	220
36	40	16	28	100	248	208	252	164	120	16	84	228	8	16	116
37	248	240	228	101	8	176	4	165	120	240	164	229	8	144	28
38	24	48	12	102	136	16	100	166	216	240	244	230	248	176	220
39	8	48	4	103	168	16	4	167	248	80	228	231	216	80	76
40	8	48	20	104	248	112	92	168	24	16	188	232	216	16	60
41	24	48	20	105	248	112	84	169	40	48	4	233	72	16	124
42	24	48	4	106	40	16	188	170	248	144	92	234	216	80	116
43	56	16	4	107	248	112	124	171	248	144	108	235	248	80	180
44	232	16	4	108	56	240	76	172	248	112	148	236	216	80	100
45	248	16	148	109	72	240	68	173	248	80	252	237	136	16	44
46	248	48	76	110	120	16	100	174	24	80	4	238	72	240	156
47	88	16	4	111	248	80	60	175	24	80	12	239	8	16	76
48	72	16	4	112	248	112	108	176	168	16	28	240	248	16	188
49	248	16	140	113	248	16	252	177	200	16	12	241	152	16	180
50	8	48	28	114	248	112	100	178	248	48	52	242	56	16	140
51	216	16	4	115	136	240	140	179	248	144	76	243	56	240	100

Table 1. (*Continued*)

Color	R	B	G	Color	R	B	G	Color	R	B	G	Color	R	B	G
52	248	48	68	116	168	16	148	180	248	144	84	244	216	48	132
53	104	16	4	117	40	16	196	181	248	144	132	245	200	16	84
54	248	144	252	118	40	16	212	182	248	48	204	246	8	16	148
55	136	16	92	119	120	240	156	183	120	240	148	247	248	16	172
56	8	112	4	120	184	16	164	184	168	16	68	248	216	16	196
57	8	16	44	121	248	208	236	185	8	16	204	249	40	80	172
58	248	16	156	122	56	240	180	186	56	16	172	250	248	112	164
59	248	208	244	123	56	16	196	187	120	16	108	251	216	16	180
60	8	80	4	124	248	112	76	188	232	208	244	252	184	16	44
61	248	80	76	125	248	48	132	189	248	80	52	253	248	112	196
62	40	16	252	126	248	80	140	190	248	48	92	254	216	16	164
63	248	176	244	127	8	48	36	191	8	208	12	255	248	176	60

work has identified a threshold for the composite beyond, which it can suffer, sever damage and its mechanical properties can be markedly affected. Table 1 shows the effect of impact energy on the tensile strength of the 5 mm thick RIM samples. Figure 8 shows a doubly impacted RIM sample with 28.6 J and 42.6 J. This is carried out to physically compare damaged propagation and sample response to multiple inputs.

5. Discussion and Analysis

Time Video Thermography (TVT) consists of heating the specimen and then recording the temperature decay curve. Qualitatively, the phenomenon is as follow. The material changes over time after the initial thermal pulse because the thermal front propagates, by diffusion, under the surface and because of radiation and convection losses. The presence of a defect reduces the diffusion rate so that when observing the surface temperature, defects appear as areas of different temperatures with respect to surrounding sound areas once the thermal front has reached them. Consequently, deeper defects will be observed later and with a reduced contrast.

Taking into consideration the discussed mathematical and behavioral models, and considering Tables 1–4, we can produce a

Table 2. RGB data for Fig. 6.

Color	R	B	G	Color	R	B	G	Color	R	B	G	Color	R	B	G
0	8	16	4	64	184	16	4	128	72	16	44	192	88	80	68
1	136	16	4	65	8	80	20	129	72	80	52	193	88	112	100
2	0	0	128	66	200	16	4	130	104	144	108	194	104	16	76
3	128	0	128	67	40	48	20	131	136	176	124	195	104	144	92
4	0	128	0	68	168	16	4	132	248	208	220	196	104	80	148
5	128	128	0	69	24	80	4	133	248	176	244	197	104	144	148
6	0	128	128	70	8	16	60	134	8	16	76	198	120	112	116
7	192	192	192	71	248	208	244	135	24	144	4	199	120	112	140
8	200	208	220	72	248	208	236	136	40	80	12	200	136	16	12
9	168	240	204	73	24	48	36	137	40	48	44	201	136	16	52
10	8	16	132	74	40	80	4	138	56	112	20	202	136	144	108
11	136	16	132	75	8	112	20	139	56	16	44	203	136	176	132
12	8	144	4	76	216	240	236	140	56	16	52	204	152	16	52
13	136	144	4	77	216	16	4	141	56	48	60	205	152	144	156

Table 2. (*Continued*)

Color	R	B	G	Color	R	B	G	Color	R	B	G	Color	R	B	G
14	8	144	132	78	8	80	36	142	56	80	60	206	168	16	28
15	200	208	196	79	56	16	20	143	72	16	20	207	168	48	156
16	8	16	12	80	8	48	36	144	104	80	60	208	168	176	156
17	24	16	12	81	40	48	28	145	120	112	108	209	200	176	164
18	24	16	20	82	40	16	44	146	120	112	132	210	8	16	100
19	8	16	20	83	56	48	4	147	184	16	20	211	8	16	108
20	24	16	28	84	56	16	28	148	232	16	4	212	24	112	36
21	8	16	28	85	200	16	12	149	248	208	212	213	24	80	44
22	24	16	4	86	216	240	252	150	8	16	92	214	24	48	52
23	232	240	244	87	248	176	252	151	24	112	4	215	40	112	4
24	232	240	236	88	8	112	36	152	24	112	12	216	40	16	52
25	248	240	244	89	24	16	52	153	24	16	68	217	40	80	60
26	248	240	236	90	72	48	4	154	40	48	52	218	232	112	156
27	232	240	252	91	200	16	20	155	40	16	60	219	184	208	180
28	40	16	12	92	24	80	20	156	56	80	20	220	168	80	116
29	248	240	252	93	56	80	4	157	56	112	36	221	168	16	76
30	40	16	20	94	8	112	12	158	56	240	172	222	136	144	204
31	24	16	36	95	216	240	244	159	72	48	60	223	136	112	68
32	8	16	36	96	232	208	252	160	72	80	60	224	136	16	68
33	40	16	4	97	248	240	212	161	120	16	92	225	120	208	100
34	40	16	28	98	248	208	228	162	120	112	124	226	72	144	76
35	24	48	12	99	8	80	44	163	120	176	124	227	72	240	76
36	8	48	12	100	40	80	20	164	136	144	116	228	88	240	164
37	8	48	20	101	72	16	12	165	152	144	132	229	88	48	116
38	8	48	4	102	8	16	68	166	152	144	148	230	56	80	108
39	24	48	20	103	24	80	28	167	168	48	28	231	72	48	132
40	248	240	228	104	200	16	28	168	184	16	12	232	72	48	148
41	24	48	4	105	8	112	28	169	216	240	196	233	72	176	100
42	8	48	28	106	24	80	12	170	216	240	212	234	72	16	92
43	56	16	4	107	232	240	220	171	216	240	228	235	56	16	108
44	8	16	44	108	232	208	244	172	232	208	236	236	72	144	116
45	72	16	4	109	8	48	44	173	8	144	20	237	8	16	196
46	88	16	4	110	24	80	36	174	8	176	36	238	104	16	60
47	232	240	228	111	40	80	28	175	24	16	60	239	104	144	60
48	24	48	28	112	40	48	36	176	40	80	52	240	120	80	92
49	8	80	4	113	40	80	44	177	40	80	68	241	248	176	68
50	24	16	44	114	56	16	36	178	40	16	76	242	248	48	68
51	40	16	36	115	72	16	68	179	40	80	76	243	200	112	172
52	8	16	52	116	88	16	20	180	56	48	36	244	184	144	140
53	248	240	220	117	184	16	28	181	56	112	44	245	184	144	124
54	120	16	4	118	216	16	12	182	56	48	52	246	168	176	196
55	104	16	4	119	216	208	252	183	56	80	52	247	168	112	188
56	152	16	4	120	248	240	196	184	72	80	4	248	152	144	172
57	40	48	4	121	248	240	204	185	72	16	28	249	152	80	140
58	40	48	12	122	8	144	12	186	72	16	76	250	136	16	28
59	248	208	252	123	8	16	84	187	72	80	76	251	88	16	180
60	8	112	4	124	24	48	44	188	72	80	92	252	56	48	164
61	8	80	12	125	40	80	36	189	72	16	204	253	8	208	4
62	8	80	28	126	56	48	20	190	88	48	4	254	152	208	172
63	56	16	12	127	56	112	52	191	88	16	44	255	136	208	148

Table 3. RGB data for Fig. 7.

Color	R	B	G	Color	R	B	G	Color	R	B	G	Color	R	B	G
0	8	16	4	64	40	48	20	128	216	240	204	192	200	240	228
1	136	16	4	65	248	208	252	129	232	208	228	193	8	48	52
2	0	0	128	66	40	48	4	130	8	144	20	194	24	144	4
3	128	0	128	67	56	16	12	131	8	112	36	195	24	112	12
4	0	128	0	68	184	16	4	132	24	80	28	196	40	112	36
5	128	128	0	69	8	16	52	133	56	48	28	197	56	80	12
6	0	128	128	70	200	16	4	134	56	48	44	198	56	48	36
7	192	192	192	71	216	240	244	135	56	16	60	199	56	16	76
8	200	208	220	72	24	80	12	136	72	16	36	200	56	112	76
9	168	240	204	73	216	16	4	137	72	16	52	201	72	80	28
10	8	16	132	74	216	240	252	138	72	48	52	202	72	240	84
11	136	16	132	75	8	80	36	139	88	16	52	203	88	80	76
12	8	144	4	76	56	16	20	140	120	16	84	204	88	144	92
13	136	144	4	77	8	16	60	141	152	16	20	205	104	48	4
14	8	144	132	78	24	80	20	142	184	16	28	206	104	48	84
15	200	208	196	79	248	208	244	143	200	16	12	207	104	112	100
16	24	16	12	80	216	240	228	144	232	240	212	208	104	144	108
17	8	16	12	81	248	208	236	145	248	240	212	209	120	16	20
18	8	16	20	82	40	80	4	146	248	208	228	210	120	48	76
19	24	16	20	83	40	48	28	147	40	80	12	211	120	144	116
20	24	16	28	84	232	208	244	148	40	80	52	212	136	16	20
21	8	16	28	85	40	16	44	149	56	80	28	213	136	112	124
22	24	16	4	86	56	48	4	150	56	16	52	214	136	144	132
23	232	240	244	87	232	208	252	151	56	48	52	215	152	16	36
24	248	240	244	88	40	16	52	152	72	80	4	216	152	144	124
25	232	240	236	89	56	80	4	153	72	16	12	217	152	240	132
26	248	240	236	90	8	112	12	154	72	16	68	218	184	240	196
27	232	240	252	91	8	16	68	155	104	16	36	219	232	208	220
28	40	16	12	92	24	48	36	156	104	144	116	220	248	176	236
29	248	240	252	93	56	16	28	157	120	16	92	221	8	144	28
30	40	16	20	94	248	240	220	158	120	16	100	222	8	80	60
31	24	16	36	95	40	48	44	159	136	240	148	223	8	80	68
32	8	16	36	96	72	48	4	160	168	16	28	224	8	112	76
33	40	16	4	97	8	112	20	161	216	240	212	225	248	80	76
34	24	48	12	98	8	48	44	162	216	208	244	226	216	112	244
35	8	48	12	99	40	80	20	163	8	112	44	227	200	144	204
36	40	16	28	100	200	16	20	164	8	16	76	228	184	144	140
37	8	48	20	101	8	112	28	165	8	16	84	229	168	208	180
38	24	48	20	102	8	80	44	166	8	16	108	230	168	80	164
39	8	48	4	103	24	112	4	167	24	112	20	231	56	80	148
40	8	48	28	104	40	48	36	168	40	112	4	232	56	240	164
41	24	48	4	105	72	16	28	169	40	112	44	233	72	144	4
42	56	16	4	106	216	240	220	170	40	48	52	234	168	80	148
43	232	240	228	107	232	16	4	171	56	80	44	235	152	144	188
44	24	48	28	108	232	240	220	172	72	16	20	236	152	240	164
45	248	240	228	109	8	l44	12	173	72	48	44	237	152	176	108
46	8	80	4	110	24	80	44	174	72	80	68	238	152	16	68
47	72	16	4	111	40	80	36	175	72	240	68	239	88	240	164
48	8	16	44	112	216	16	12	176	72	240	76	240	136	144	172
49	88	16	4	113	8	80	52	177	88	16	20	241	136	112	76
50	24	16	44	114	56	48	20	178	88	112	92	242	120	176	156
51	8	80	20	115	184	16	12	179	104	16	12	243	104	80	60

Table 3. (*Continued*)

Color	R	B	G	Color	R	B	G	Color	R	B	G	Color	R	B	G
52	104	16	4	l16	248	176	252	180	104	16	20	244	88	112	140
53	8	48	36	117	24	16	52	181	104	80	116	245	72	16	100
54	168	16	4	118	40	80	28	182	104	112	116	246	88	16	180
55	8	80	12	119	56	16	36	183	120	112	92	247	56	48	244
56	40	48	12	120	56	16	44	184	120	80	108	248	8	208	20
57	40	16	36	121	216	208	252	185	120	176	132	249	8	208	4
58	8	80	28	122	232	208	236	186	136	16	44	250	248	144	84
59	152	16	4	123	24	80	36	187	136	48	92	251	184	144	188
60	8	112	4	124	24	16	60	188	152	112	116	252	168	176	156
61	24	80	4	125	56	48	12	189	200	16	28	253	168	16	52
62	120	16	4	126	56	80	60	190	200	240	196	254	152	144	92
63	216	240	236	127	72	112	108	191	200	240	220	255	136	112	156

Table 4. RGB data for Fig. 8.

Color	R	B	G	Color	R	B	G	Color	R	B	G	Color	R	B	G
0	8	16	4	64	152	16	4	128	248	16	100	192	120	240	140
1	136	16	4	65	248	176	244	129	248	80	148	193	120	80	132
2	8	16	132	66	248	144	236	130	248	144	212	194	168	48	164
3	136	16	132	67	8	112	12	131	248	80	220	195	184	16	148
4	8	144	4	68	248	176	236	132	8	144	28	196	168	176	164
5	136	144	4	69	8	112	20	133	24	112	20	197	184	16	132
6	8	144	132	70	40	48	20	134	24	80	36	198	168	80	148
7	200	208	196	71	56	16	12	135	40	16	44	199	200	16	68
8	200	208	220	72	200	16	4	136	56	80	28	200	56	112	76
9	168	240	204	73	248	176	252	137	56	16	44	201	216	16	92
10	8	16	28	74	24	80	12	138	88	16	196	202	88	16	108
11	8	16	60	75	248	176	228	139	104	240	164	203	88	80	4
12	8	16	84	76	8	80	36	140	200	16	20	204	248	16	60
13	8	16	116	77	40	48	12	141	216	240	244	205	72	240	188
14	8	16	140	78	56	16	20	142	248	16	76	206	248	112	100
15	8	16	172	79	248	144	220	143	248	48	76	207	72	112	148
16	24	16	12	80	248	208	220	144	248	112	132	208	72	16	76
17	8	16	12	81	8	112	28	145	248	48	148	209	72	16	60
18	24	16	20	82	8	16	52	146	248	80	164	210	248	240	180
19	8	16	20	83	184	16	4	147	248	176	196	211	56	80	172
20	24	16	28	84	216	16	4	148	8	80	52	212	40	16	124
21	24	16	4	85	24	80	4	149	8	16	92	213	40	16	68
22	232	240	244	86	40	48	4	150	24	48	44	214	8	240	164
23	248	240	244	87	232	208	244	151	232	16	4	215	8	80	140
24	248	240	236	88	24	80	28	152	232	240	220	216	248	240	156
25	232	240	236	89	248	144	252	153	248	48	124	217	248	176	76
26	232	240	252	90	8	112	36	154	248	48	140	218	152	240	140
27	248	240	252	91	24	80	20	155	248	112	188	219	136	240	156
28	40	16	12	92	24	48	36	156	248	112	204	220	216	16	116
29	40	16	20	93	248	112	244	157	248	112	212	221	152	16	92
30	8	16	36	94	248	144	244	158	248	176	212	222	200	80	84
31	24	16	36	95	8	144	12	159	248	48	244	223	168	80	108
32	8	48	12	96	248	176	220	160	248	48	252	224	168	16	68
33	40	16	4	97	248	80	236	161	8	176	4	225	152	48	28

Table 4. (*Continued*)

Color	R	B	G	Color	R	B	G	Color	R	B	G	Color	R	B	G
34	8	48	20	98	8	80	44	162	8	176	12	226	136	16	164
35	24	48	12	99	248	112	236	163	8	16	76	227	248	80	60
36	24	48	20	100	24	16	52	164	40	80	12	228	136	48	68
37	40	16	28	101	248	240	212	165	56	16	36	229	104	16	132
38	8	48	4	102	40	48	28	166	104	16	156	230	104	112	108
39	8	48	28	103	200	16	12	167	120	16	92	231	88	80	212
40	248	240	228	104	8	48	44	168	120	144	148	232	88	16	212
41	8	80	4	105	8	16	68	169	152	16	148	233	248	16	196
42	56	16	4	106	56	16	28	170	200	16	28	234	88	16	172
43	24	48	4	107	248	80	212	171	248	80	84	235	72	176	100
44	8	80	20	108	248	80	228	172	248	80	124	236	72	176	84
45	72	16	4	109	248	112	228	173	248	48	156	237	56	240	164
46	8	16	44	110	8	144	36	174	248	112	156	238	8	80	68
47	24	48	28	111	88	80	76	175	248	80	180	239	8	240	28
48	248	208	236	112	88	80	84	176	248	48	212	240	248	176	172
49	8	80	12	113	232	208	252	177	248	16	220	241	200	16	52
50	88	16	4	114	248	240	204	178	248	48	228	242	184	16	100
51	8	112	4	115	8	144	20	179	248	144	228	243	168	112	132
52	248	208	244	116	72	80	76	180	248	80	244	244	168	16	116
53	232	240	228	117	248	208	212	181	8	176	20	245	136	12	172
54	104	16	4	118	8	112	44	182	8	176	28	246	136	16	44
55	248	208	252	119	24	112	4	183	40	80	28	247	56	48	92
56	8	80	28	120	40	80	4	184	40	48	36	248	72	16	156
57	8	48	36	121	56	80	4	185	40	80	36	249	72	240	76
58	120	16	4	122	72	16	12	186	56	48	4	250	8	144	68
59	40	16	36	123	72	16	28	187	72	80	68	251	216	16	164
60	248	208	228	124	216	240	252	188	72	240	148	252	88	240	124
61	24	16	44	125	232	208	236	189	104	80	148	253	216	16	140
62	168	16	4	126	232	176	244	190	104	112	60	254	120	16	28
63	248	240	220	127	248	48	92	191	120	16	108	255	104	144	124

Table 5. Relationship between pixel re-grouping and impact damage.

Sample	Number of Re-grouped pixels
Reference (zero impact)	29 267
28.6 J impact	15 510
42.6 J impact	23 096
28.6 J & 42.6 J impacts	23 467
55.6 J impact (fiber breakage)	27 283

pixel-regrouping table (Table 5), is used to validate the theoretical considerations:

From the obtained images and Table 5 the following can be stated:

(i) The initial reference value indicates a near perfect sample.

(ii) At low impact energy, the re-grouped pixels represent a small damaged area.

(iii) As the impact energy increases, the damage propagates such that the number of re-grouped pixels that share common features increases.

(iv) When the impact energy exceeds the sample threshold (function of sample thickness and fiber orientation), the total number of pixels sharing similar features (damaged) will increase and start to approach the original number of undamaged pixels.

From Table 5 and taking into consideration the derived mathematical equations, we obtain the following:

(i) When there is little or no damage:
Number of regrouped pixels will almost equal to the original number 29 267/

29 267 = 1 which is consistent with $\boldsymbol{t_r} \gg \boldsymbol{t_d}$ and $\lim_{t_d \to 0} k = 1$.

(ii) When there is damage and $\boldsymbol{t_r} \cong \boldsymbol{t_d}$:
15 510/29 267 = 0.53, and $\lim_{t_d \to t_r} k = 0.5$.

(iii) When the damage is severe then $\boldsymbol{t_r} \ll \boldsymbol{t_d}$:
The response depends on both $\boldsymbol{t_r}$ and $\boldsymbol{t_d}$ and might approach one if total damage occurs to the sample:
27 283/29 267 = 0.93.

These above observations are consistent with the developed mathematical model.

From Table 5 we notice an initial decrease in the pixel regrouping value due to 28.6 J impact. This is expected, as the damaged area will serve to decrease pixel regrouping for similar levels. However, the regrouping number increases as the impact energy increased using either multiple impacts (28.6 J and 42.6 J) or increase the level of a single impact (42.5 J, 55.6 J). This steady increase in the re-grouping number to reach comparable value to the reference sample as the fiber starts to break is another proof to the validity of the mathematical model, which this work developed. When impact level increases beyond a certain threshold and causes total failure in the component, the pixel regrouping returns to a similar value to the reference non-damaged component as almost the whole of the sample becomes damaged, which reduces the differential between damaged and undamaged areas significantly. This behavior is realized and noted in this paper under what we call Closed Ring model and shown in Fig. 9.

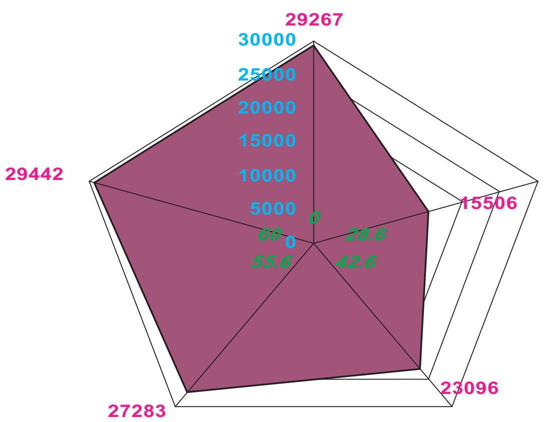

Fig. 9. Closed ring model.

Table 6. Relationship between impact energy and tensile strength for the tested RIM composites

Impact Energy (J)	Tensile Strength (N/mm^2)
Reference (Zero Impact)	208.29
14.3	206.82
28.6	205.68
42.6	180.91
55.6	153.48

Table 6 further supports our model and the reviewed literature, as it shows a decrease in the tensile strength due to increase in impact energy to reach a very low level at 55.6 J.

6. Conclusion and Future Work

The TVT technique and the established Closed Ring (CR) model can be used as a viable alternative or screening procedure for the traditional NDT methods. It can detect the same type of defects but does not require two-sided access, typically has a fast area scan rate, and can be non-contact. A test specimen is pulsed with a low heat source to create a traveling temperature gradient within the test specimen. Flaws or irregularities alter the flow of heat, producing temperature contrasts at the surface that are video captured via computer. TVT technique can then be applied to the surface image to characterize the flaw and predict performance capability [Trétout *et al.*, 1994; Hagan *et al.*, 1996; Santey & Almond 1997; Bison *et al.*, 1998; Maldague & Largouët, 1998].

The development of a TVT computer workstation using off-the-shelf components would have the benefits of low cost, ease of use, portability, and flexibility of application.

In this paper a new techniques and model is provided and validated. This innovated technique is capable of fast analysis of captured TVT images and other image formats, with smart engine based on feature extraction and Neural Networks adding the advantage of damage prediction. Further development of the system is possible to improve its accuracy and widen its range of applications [Foucher, 1999;

d'Ambrosio *et al.*, 1995; Sakagami & Kubo, 1999].

References

Balageas, D. and Levesque, P. [1998] EMIR: A photothermal tool for electromagnetic phenomena characterization, *Rev. Gén. Therm.* **37**, 725–739.

Bison, P., Marinetti, S., Manduchi, G. and Grinzato, E. [1998] "Improvement of neural networks performances in thermal NDE," *American Soc. of Non-Destructive Testing Press* **3**, 221–227.

Busse, G. [1994] "Non-destructive evaluation of polymer materials," *NDT & E Int'l* **27**(5), 253–262.

Busse, G., Wu, D. and Karpen, W. [1992] "Thermal wave imaging with phase sensitive modulated thermography," *J. Appl. Phys.* **71**(8), 3962–3965.

d'Ambrosio, G., Massa, R. and Migliore, M. [1995] "Microwave excitation for thermographic NDE: An experimental study and some theoretical evaluations," *Materials Evaluation* **53**(4), 502–508.

Dillenz, A., Zweschper, T., Riegert, G. and Busse G. [2003] "Progress in phase angle thermography," *Review of Scientific Instruments* **74**(1), 417–419.

Dinwiddie, R. and Blau, P. [1999] "Time-resolved tribo-thermography," in *Thermosense XXI, Proc. SPIE*, R. N. Wurzbach and D. D. Burleigh (eds.) **3700**, 358–368.

Favro, L. D., Han, X., Ouyang, Z., Sun, G., Sui, H. and Thomas, R. L. [2000] "Infrared imaging of defects heated by a sonic pulse," *Rev. Sci. Inst.* **71**(6), 2418–2421.

Foucher, B. [1999], "Infrared machine vision," in *Thermosense XXI, Proc. SPIE*, R. N. Wurzbach and D. D. Burleigh (eds.) **3700**, 210–213.

Galmiche, F., Maldague, X., Valler, S. and Couturier, J.-P. [2000] "Pulsed phase thermography with the wavelet transform," *AIP Conference Proceedings* **509**(1), 609–616.

Hagan, M., Demuth, H. and Beale, M. [1996] *Neural Networks Design*, PWS Publishing Company.

Huang, J., Que, P. W. and Jin, J. H. [2004] "Adaptive dynamic focusing system for ultrasonic nondestructive testing of pipeline girth welds," *Rev. Sci. Inst.* **75**(5), 1341–1346.

Maldague, X., Galmiche, F. and Ziadi, A. [2002] "Advances in pulsed phase thermography," *Infrared Physics and Technology* **43**, 175–181.

Maldague, X. and Largouët, Y. [1998] "Depth study in pulsed phase thermography using neural networks: Modeling, noise, experiments," *Revue Générale de Thermique* **37**(8), 704–708.

Maldague, X. and Marinetti, S. [1996] "Pulse phase infrared thermography," *J. Appl. Phys.* **79**(5), 2694–2698.

Osiander, R. and Spicer J. W. M. [1998] "Time-resolved infrared radiometry with step heating," *A Review, Applied Physics Laboratory* **37**(8), 680–692.

Prabhu, D., Howell, P., Syed, H. and Winfree, W. [1992] *Application Artificial Neural Networks to Thermal Detection of Disbands*, pp. 1331–13382.

Rantala, J., Wu, D. and Busse, G. [1996] "Amplitude modulated lock-in vibrothermography for NDE of polymers and composites," in *Research in NDE* **7**, 215–228.

Sakagami, T. and Kubo, S. [1999] "Proposal of a new thermographical non-destructive testing technique using microwave heating," in *Thermosense XXI, Proc. SPIE*, R. N. Wurzbach and D. D. Burleigh (eds.) **3700**, 99–103.

Salerno, A., Wu, D., Busse, G. and Rantala, J. [1996] "Thermographic inspection with ultrasonic excitation," in *Proc. of Rev. Progresses in Quantitat. NDE*, D. O. Thompson and D. E. Chimenti (eds.), NY, Plenum Press **16A**, 5–352.

Santey, M. B. and Almond, D. P. [1997] "An artificial neural network interpreter for transient thermography image data," *NDT & E Int.* **30**(5), 291–295.

Spicer, J. W. M., Wilson, D. W., Osiander, R., Thomas, J. and Oni, B. O. [1999] "Evaluation of high thermal conductivity graphite fibers for thermal management in electronics applications," in *Thermosense XXI, Proc. SPIE*, R. N. Wurzbach and D. D. Burleigh (eds.) **3700**, 40–47.

Tenek, L. H. and Henneke, E. G. [1991] "Flaw dynamics and vibro-thermographic thermoelastic NDE of advanced composite materials," in *Thermosense XIII, Proc. SPIE*, G. S. Baird (ed.) **1467**, 252–263.

Trétout, H., David, D., Marin, J. and Dessendre, M. [1994] "An evaluation of artificial neural networks applied to infrared thermography inspection of composite aerospace structures," *Review of Progress in Quantitative NDE*, D. O. Thompson and D. E. Chimenti (eds.) **14**, 827–834.

Wu, D., Salerno, A., Malter, U., Aoki, R., Kochendrfer, R., Kächele, P., Woithe, P. K., Pfister, K. and Busse, G. [1996] "Inspection of aircraft structural components using lockin-thermography," *QIRT-96* (*Quantitative Infrared Thermography*), *Eurotherm Seminar 50*, D. Balageas, G. Busse and C. Carlomagno (eds.) Edizioni ETS (Pisa, Italy), pp. 251–256.

Biography

Mahmoud Iskandarani received the BEng (Hons) degree in electronics engineering, the MSc degree in engineering (analogue neural processor) and the PhD in engineering (smart classification and neural networks) from the University of Warwick, UK. He has obtained a certificate in Non-Destructive Testing from the University of London as well as the Networking Certificate from the Royal Scientific Society in Jordan. His research interests include neural networks, artificial intelligence, smart systems and biometrics.

Nidal Shilbayeh received the BS degree in computer science from Yarmouk University, Irbid, Jordan in 1988, the MS degree in computer science from Montclair State University, New Jersey, USA in 1992, and the PhD in computer science from Rajesthan University, Rajesthan, India in 1997. He is an associate professor and head of the computer science department at Applied Science University. His research interests include embedding, nose system, neural network, image processing, and pattern recognition.